Appl. Phys. B 81, 101–111 (2005)
DOI: 10.1007/s00340-005-1852-z

Applied Physics B
Lasers and Optics

A. STAMPANONI-PANARIELLO[1]
D.N. KOZLOV[2]
P.P RADI[3], ✉
B. HEMMERLING[3]

Gas phase diagnostics by laser-induced gratings I. theory

[1]Institute for Quantum Electronics, ETH Zürich, 8093 Zürich, Switzerland
[2]A.M. Prokhorov General Physics Institute, 119991 Moscow, Russia
[3]Paul Scherrer Institute, 5232 Villigen PSI, Switzerland

Received: 15 April 2005
Published online: 3 June 2005 •

ABSTRACT Electrostriction and collisional thermalization of absorbed laser energy are the two dominant mechanisms leading to the formation of laser-induced gratings (LIGs) in the gas phase. In this article the results of the theoretical investigations that have been achieved in the past ten years at the Paul Scherrer Institute on this issue are summarized and yield a comprehensive understanding of the underlying physical concepts. Furthermore, a study of the influence of various parameters, such as the alignment and the spatial intensity profile of the beams on the generated electrostrictive and thermal signal is presented for the first time to the authors' knowledge. The variations of the refractive index responsible for the appearance of laser-induced gratings have been theoretically described by solving the linearized hydrodynamic equations. The contributions from electrostriction, as well as from instantaneous and slow relaxation of the absorbed radiation energy into heat is obtained. These expressions are employed for analysis of experimental data presented in the companion paper [1] which is devoted to the application of the technique for diagnostic purposes in the gas phase. Much effort has been undertaken in order to allow a straightforward physical interpretation of the experimental findings of the expressions presented here.

PACS 42.62.-b; 43.35.+d; 42.65.Es

1 Introduction

Laser-induced gratings (LIGs) arise from the nonlinear interaction between a medium and the radiation of an interference structure generated by two crossed laser beams. The interference produces a spatially periodic light intensity and/or polarization distribution which changes the optical properties (e.g., refractive index and absorption coefficient) of a material placed into the overlap region of the beams. The spatially periodic modulation of the complex refractive index acts thus as a phase or amplitude grating in the diffraction of incident probe light [2]. Diffraction of light from the modulations of the optical properties of a material caused by the presence of a radiation field is referred to as stimulated, or forced light scattering [3]. The formation of dynamic laser induced gratings occurs by various resonant or nonresonant light-matter interaction mechanisms. In the gas phase the dominant grating formation processes are electrostriction and heat exchange with a thermal bath in the course of collisional relaxation of the absorbed laser energy. Other effects like photophoresis and thermophoresis are of minor importance. Optical gratings generated by electrostriction and collisional relaxation of the absorbed laser radiation are referred to as electrostrictive and thermal gratings, respectively. The mechanisms leading to the formation of thermal and of electrostrictive LIGs are fundamentally different. The physical phenomenon underlying the formation of thermal gratings is light absorption followed by collisional relaxation. Initially, the laser radiation is absorbed by the molecules through electronic (and/or vibrational) transitions of the medium. More precisely, a spatially periodic modulation of the population, reflecting the intensity distribution of the interference structure, is formed in the ground and the excited state, respectively. Such a spatially periodic modulation of the population is referred to as population grating [2]. Subsequent thermalization of the absorbed laser energy through collisions leads to temperature and hence to density variations within the medium. The time scale of the energy exchange between the excited molecules and the surrounding medium will determine the nature of the thermal grating. If this energy exchange is sufficiently fast it drives acoustic waves, otherwise an isobaric stationary density variation is generated. The process of light scattering by the density variations from fast energy exchange is referred to as stimulated thermal Brillouin scattering (STBS) [3]. Light scattering by the stationary density modulations is referred to as stimulated thermal Rayleigh scattering (STRS) [3].

The process leading to the formation of electrostrictive gratings is electrostriction, which is the tendency of a material to vary its density in presence of an electric field. Unlike thermal gratings, electrostrictive gratings are generated at any frequency of the employed laser light. The electric field of the interference structure polarizes the dielectric medium, and the spatial inhomogeneity of the electric field leads to a motion of mass. If this motion is rapid acoustic waves are formed eventually. Constructive interference of the acoustic waves occurs only in a direction normal to the planes of the fringes. Thus, two counter-propagating acoustic waves are

✉ Fax: +41-1-633-13-54, E-mail: radi@phys.ethz.ch

formed, with their wavelength defined by the fringe spacing of the interference pattern. Two counter-propagating acoustic waves form a standing acoustic wave and thereby a spatial, time-dependent density modulation. The variation of density, associated with an acoustic wave (i.e., the adiabatic density modulation), causes a variation of the real part of the complex refractive index which acts as a phase grating. The signal beam obtained by diffraction of a probe beam off this grating is modulated in time by the evolution of the laser-induced perturbation. Light diffraction from electrostrictive gratings is analogous to the STBS effect and is referred to as electrostrictive stimulated Brillouin scattering (SBS) [3].

This article together comprises the results of the theoretical investigations achieved in the past ten years at the Paul Scherrer Institute of Villigen (Switzerland) see [4–6]. In the following an outline of the topics dealt with in this work is given. In Sect. 2, the linearized hydrodynamic equations are solved to obtain an expression for the laser-induced density variations caused by electrostriction and thermalization of absorbed laser energy. The full calculations are presented in [7] and the references therein. The expressions presented here allow for a more straightforward and intuitive physical interpretation compared to the expressions presented so far in [4–6]. In Sect. 3 the influence of various parameters such as the alignment and spatial intensity profile of the beams on the generated electrostrictive and thermal LIGs is shown for the first time to the author's knowledge. In particular, the coherence length of the output of the multimode, pulsed laser source has been measured by using electrostrictive laser-induced gratings. Furthermore, the potential of laser induced gratings for the investigation of optical breakdown in gases is qualitatively shown. All these investigations provide a test for the theoretical model and allow one to select the best matching experimental configuration for the measurement of the desired parameters. The experiments presented in [1] have been designed based on these findings.

2 Theoretical considerations

Laser-induced gratings are formed in a medium by various resonant and non-resonant mechanisms as response to the spatially periodic modulated light field generated by the interference of two excitation beams with electric fields $\mathbf{E_1}(\mathbf{r},t)$ and $\mathbf{E_2}(\mathbf{r},t)$. These two light waves are assumed to be parallel polarized monochromatic plane waves, perfectly coherent. Since the duration of the excitation pulses is small compared to the other characteristic times in our experiments, their temporal shape can be approximated by a δ-function at $t = t_0$. The calculation for pulses displaying a Gaussian temporal shape is given at the end of this section.

It is the spatially periodic modulated part $\mathbf{E_s}$ of the total electric field $\mathbf{E}(\mathbf{r},t)=\mathbf{E_1}(\mathbf{r},t)+\mathbf{E_2}(\mathbf{r},t)$ of the interference structure, averaged over an optical period (denoted by the bar sign over E_s^2), that leads to the grating formation, i.e.,

$$\bar{E}_s^2 = 2A\cos(qx)\,\delta(t-t_0)\,. \tag{1}$$

The spatially constant field $E^2 - E_s^2$ is neglected in Eq. (1): it gives rise to an overall temperature variation which is included in a redefined undisturbed value of the temperature T_0. In Eq. (1) A denotes a real constant which is proportional to the excitation pulses energies, and is given by

$$A = \frac{1}{nS}\sqrt{\frac{\mu_0}{\varepsilon_0}W_1 W_2} \tag{2}$$

where, n is the refractive index, S is the cross section of the beams in their overlap region, W_1, W_2 are the pulse energies of the excitation beams. The coordinate x points along the direction perpendicular to the line bisecting the intersection angle of the two laser beams. The interference fringe pattern is characterized by a grating vector $\mathbf{q}$

$$\mathbf{q} = \pm\left(\mathbf{k}_{\mathbf{E}_1} - \mathbf{k}_{\mathbf{E}_2}\right), \tag{3}$$

where $\mathbf{k}_{\mathbf{E}_1}$ and $\mathbf{k}_{\mathbf{E}_2}$ denote the wave vectors of the excitation beams. The length of the grating vector, $q = |\mathbf{q}|$, is related to the fringe spacing Λ of the interference pattern according to

$$q = \frac{2\pi}{\Lambda}, \tag{4}$$

where

$$\Lambda = \frac{\lambda_{\mathrm{exc}}}{2\sin\left(\frac{\theta}{2}\right)}. \tag{5}$$

Here, λ_{exc} denotes the wavelength of the excitation laser, and θ the intersection angle of the two excitation beams. The excitation beams have been assumed to be plane waves. If they have a finite cross section, the lateral extent of the interference region is limited. A calculation of this effect is given in [8] and [9].

If material is placed into the region of interference, light-matter interaction may create a corresponding spatially periodic modulation of some material characteristics, which change the optical properties. In the simplest case absorption and refraction of the material are changed resulting in amplitude and phase gratings. More precisely, the material excitation couples to the refractive index n and to the absorption coefficient α which then exhibits a grating-like modulation with amplitudes $\Delta n(\lambda_{\mathrm{pr}})$ and $\Delta\alpha(\lambda_{\mathrm{pr}})$, respectively. Both amplitudes are functions of the probing wavelength λ_{pr} of a third laser beam which is diffracted off the induced grating. Probe and excitation beams are typically of different frequency. That part of the probe beam diffracted by the grating is called the signal beam. If the grating thickness is large compared to the fringe spacing the grating can be efficiently probed only when the Bragg condition

$$\mathbf{k_{pr}} - \mathbf{k_S} = m\mathbf{q}, \quad m = \pm 1, 2, \ldots \tag{6}$$

is obeyed, where $\mathbf{k}_{\mathrm{pr}}$ and $\mathbf{k}_{\mathrm{S}}$ are the wave vectors of the probe and the signal beam, respectively. The normalized intensity of the first-order ($m = \pm 1$) diffracted beam is in first approximation, see e.g., [2]

$$\eta = \frac{I_{\mathrm{S}}}{I_{\mathrm{pr}}} = \left(\frac{\pi\,\Delta n\,d}{\lambda_{\mathrm{pr}}}\right)^2 + \left(\frac{\Delta\alpha d}{4}\right)^2 \tag{7}$$

where I_{pr} and I_{S} are the intensities of the probe beam and the diffracted beam, respectively, and d is the thickness of the grating. In absence of a molecular/atomic resonance at the wavelength of the probe laser $\Delta\alpha$ is equal to zero and a pure phase grating is obtained, whereas in the case of $\Delta n = 0$

a pure amplitude grating results. The parameter η is called diffraction efficiency of an optical grating.

In general, any light-induced modulation of a material property with amplitude ΔX inside a medium will be accompanied by an optical grating with an amplitude [2]

$$\Delta \mathbf{n} = \left(\frac{\partial \mathbf{n}}{\partial X}\right) \Delta X. \tag{8}$$

The light-induced modulation of the complex refractive index $\mathbf{n}= n+i\alpha$ due to electrostriction and to collisional relaxation of the absorbed laser radiation can be expressed as

$$\Delta \mathbf{n} = \left(\frac{\partial \mathbf{n}}{\partial N_{ij}}\right) \Delta N_{ij} + \left(\frac{\partial \mathbf{n}}{\partial T}\right)_{\rho} \Delta T + \left(\frac{\partial \mathbf{n}}{\partial \rho}\right)_{T} \Delta \rho. \tag{9}$$

Here, ΔN_{ij} is the deviation from the thermal population difference between the two molecular levels i and j having an energy difference that matches the frequency of the excitation laser. The first term in Eq. (9) describes the influence of the population transfer induced by the radiation of the excitation laser on the complex refractive index. Once the absorbed energy is thermalized, the complex refractive index is a function of local thermodynamic quantities. In a gas the thermo-optic coefficient $(\partial \mathbf{n}/\partial T)$ is usually small and can be neglected in comparison to the change of the complex refractive index caused by the density perturbation [10].

In the following, the variation of the density from the initially undisturbed, spatially homogeneous value ρ_0 will be denoted ρ' (i.e., $\rho' = \rho - \rho_0$) and can be written as

$$\rho'(x,t) = \Delta\rho(t) f(x) \tag{10}$$

where, $f(x)$ contains the spatially periodic dependence of the density variation ρ'.

For the experiments described in this work, the condition of local thermal equilibrium in the medium is fulfilled, because the grating spacing is large compared to the mean free path, and the mean time between two collisions of a molecule is small compared to the pulse duration of the excitation laser and to the decay time of the acoustic wave. Thus, the density variation ρ' can be calculated by solving the linearized fluid dynamic equations [5, 10, 11]

$$-\frac{\partial^2 \rho'}{\partial t^2} + \frac{v_s^2}{\gamma}\Delta\rho' + \frac{v_s^2 \beta_p \rho_0}{\gamma}\Delta T' + \frac{\eta_{visc}}{\rho_0}\frac{\partial}{\partial t}(\Delta\rho') = \nabla \mathbf{f}_{ext}$$

$$\rho_0 c_v \frac{\partial T'}{\partial t} - \frac{c_v(\gamma-1)}{\beta_p}\frac{\partial \rho'}{\partial t} - \kappa \Delta T' = \phi_{ext}, \tag{11}$$

where η_{visc} denotes the viscosity, $v_s = (\partial p/\partial \rho)_S^{1/2}$ the adiabatic sound velocity, $\beta_p = -(1/\rho)(\partial \rho/\partial T)_p$ the thermal expansion coefficient at constant pressure, c_V the specific heat at constant volume, $\gamma = c_p/c_V$ the specific heat ratio, and κ the thermal conductivity. In Eq. system (11) the continuity equation in its linearized form has been used to eliminate the flow velocity from the equation of momentum transfer (upper equation) and from the energy transport equation (lower equation). The term f_{ext} represents the force per unit volume of any externally imposed force. If the density variation ρ' is induced by electrostriction, f_{ext} is [10]

$$f_{ext} = \frac{\varepsilon_0 \gamma_e}{2}\nabla \bar{E}_S^2, \tag{12}$$

where, $\gamma_e = \rho(\partial\varepsilon/\partial\rho)$ represents the electrostrictive coupling constant.

Release of absorbed laser light in form of heat by quenching provides the source term in the energy transport equation. Depending on the pathways of energy release ϕ_{ext} has to be modeled by a cascaded set of rate equations. If only a single step of the energy conversion process is assumed φ_{ext} can be written as [6]

$$\varphi_{ext} = \varepsilon_0 nc\lambda\zeta\alpha\ \Theta(t-t_0)\ \ \exp(-\mu(t-t_0))\,\bar{E}_s^2 \tag{13}$$

Here, μ is a decay rate that can be expressed as $\mu = \lambda + \psi$, where λ is the decay rate of the heat release from collisional de-excitation transitions between molecular internal energy levels, and ψ accounts for the wash-out of the induced population modulation caused by mass diffusion. α is the optical absorption coefficient, ζ the part of excitation energy that is released in form of heat, and Θ the Heavyside unit step function. A calculation of multiple relaxation processes with the corresponding decay rates is given in [6, 12].

Solving system Eq. (11) by taking into account only terms up to first order in β_1/ϖ and β_2/ϖ, where ϖ is the acoustic frequency, β_1 and β_2 are the decay rates, see Eq. (19) below, one obtains for the induced density variation [5–7]

$$\rho'(t,x) = \varepsilon_0 A q^2 \cos(qx)\,\Theta(t-t_0)\,(\Xi_{elect}(t) + \Xi_{therm}(t)) \tag{14}$$

where, the contribution due only to electrostriction is given by

$$\Xi_{elect}(t) \equiv \frac{\gamma_e}{\varpi}\left\{e^{-\beta_1(t-t_0)}[L\sin(\varpi(t-t_0)+\Phi)] + \xi e^{-[\beta_2(t-t_0)]}\right\} \tag{15}$$

with

$$\xi \equiv \left(\frac{\beta_2(\gamma-1)}{\varpi}\right)$$
$$L \equiv (1+\xi^2)^{1/2} \tag{16}$$
$$\Phi \equiv arctg(-\xi)$$

and where the contribution due to collisional relaxation of the absorbed laser radiation is given by

$$\Xi_{therm}(t) \equiv \frac{\zeta\gamma_a\lambda q v_s}{\varpi^3\left[1-\mu\left(\frac{2\beta_1}{\varpi^2}\right)+\left(\frac{\mu}{\varpi}\right)^2\right]} \times \left\{e^{-\beta_1(t-t_0)}(L'\sin[\varpi(t-t_0)+\Phi']) - \frac{\varpi}{\beta_2-\mu}\left[e^{-\mu(t-t_0)} - \left(1-\mu\left(\frac{2\beta_1}{\varpi^2}\right) + \left(\frac{\mu}{\varpi}\right)^2\right)e^{-\beta_2(t-t_0)}\right]\right\} \tag{17}$$

with

$$L' \equiv \left(\left(\frac{\mu\,(\beta_1 - \beta_2)}{\varpi^2} + 1 \right)^2 + \left(\frac{2\beta_1 - \beta_2 - \mu}{\varpi} \right)^2 \right)^{1/2}$$
$$\Phi' \equiv arctg \left(- \frac{\left(\frac{2\beta_1 - \beta_2 - \mu}{\varpi} \right)}{\left(\frac{\mu(\beta_1 - \beta_2)}{\varpi^2} + 1 \right)} \right) \tag{18}$$

where $\gamma_a \equiv \frac{2\alpha n c v_S \beta_P}{c_P q}$ is a dimensionless absorptive coupling constant, see [10]. In the approximation that takes into account only linear terms in β_1/ϖ and β_2/ϖ (weak damping condition) the acoustic frequency ϖ and the decay rates β_1 and β_2 can be written as [5]

$$\varpi = q v_S,$$
$$\beta_1 = \frac{q^2}{2\rho_0} \left[\eta_{visc} + \frac{(\gamma - 1)\,\kappa}{c_p} \right], \tag{19}$$
$$\beta_2 = \frac{\kappa\, q^2}{\rho_0 c_p}.$$

The temporal evolution of the density variation comprises the contributions Ξ_{elec} and Ξ_{therm}, which are due to electrostriction and collisional induced release of absorbed laser energy in form of heat.

The density variation due to electrostriction is a primarily standing acoustic wave, with its time dependence described by the first term in the curled brackets of Eq. (15). In addition to the standing acoustic wave, a stationary density modulation with small amplitude ξ is formed. Its time dependence is described by the second term in the curled bracket of Eq. (15). (Light diffraction from this density modulation is referred to as electrostrictive stimulated Rayleigh scattering). Viscosity and heat conduction damp the acoustic wave, while the stationary density modulation is damped solely by heat conduction as it results from the expression for the decay rates β_1 and β_2. For the experiments reviewed in this work the ratio of the decay constants and the generated acoustic frequencies ϖ is very small compared to 1, i.e., $\xi \ll 1$. For example, assuming a typical acoustic frequency of 50 MHz generated in air at 22°C, $\xi = 4 \times 10^{-3}$, it follows that the stationary density modulation can be neglected, while the amplitude of the standing acoustic wave is $L \approx 1$ and its phase is $\Phi \approx 0$. The density related to the standing acoustic wave oscillates in time passing through its unperturbed value twice during each acoustic period $T_a = 2\pi/q v_s = \Lambda/v_s$. The diffraction efficiency η of the grating is proportional to the squared amplitude $\Delta\rho(t)$ of the induced density variation $\rho'(\mathbf{r}, t)$

$$\eta(t) \propto \left(\gamma_e \frac{\varepsilon_0 A q^2}{\varpi} \right)^2 e^{-2\beta_1 (t - t_0)} \left(1 - \cos\left(2\varpi (t - t_0)\right)\right). \tag{20}$$

Therefore, the diffraction efficiency of a electrostrictive LIG consisting purely of acoustic waves oscillates with a period which is half the acoustic period, i.e.,

$$T_g = \frac{1}{2} T_a, \tag{21}$$

and decays at a rate $2\beta_1$. For example, the lifetime of a grating induced in air at ambient conditions with a fringe spacing $\Lambda = 41\,\mu m$ is roughly 1.5 μs.

For the derivation of Eq. system (11) linearity in the induced density variation ρ' has been assumed. In fact, for the experiments described in this work the maximum value of ρ' is small enough to justify this assumption. For example, using Eqs. (14) and (15) one obtains for the induced maximum density variation $\rho' = 1 \times 10^{-4}$ kg/m^3, which corresponds to a pressure disturbance of 6.2×10^{-5} bar. Here, we have assumed an electrostrictive grating generated in argon at 5 bar with excitation energies of roughly 90 mJ each at a wavelength of λ_{exc} =1064 nm, a beam diameter of 1 mm and an intersection angle of the excitation beams of about 1.5°.

Consider now the contribution due to collisional relaxation of the absorbed laser radiation given by Eq. (17). Depending on the sign and magnitude of the energy exchange rate μ (i.e., exo- or endothermic process and time-scale of the process, respectively) the induced density variation exhibits a completely different temporal behavior. If the absorbed energy is released into heat instantaneously, i.e., $\mu \gg \varpi$, Eq. (17) becomes

$$\Xi_{therm}(t) = \frac{\gamma_a \zeta}{\varpi} \left\{ e^{-\beta_1 (t - t_0)} \cos\left[\varpi (t - t_0)\right] - e^{-\beta_2 (t - t_0)} \right\}. \tag{22}$$

Instantaneous energy release causes, at the locations of high total field intensity, a temperature and pressure rise according to an adiabatic process. With increasing time, the acoustic energy leaves the volume leading to a pressure drop and hence to a density reduction. A standing acoustic wave and a stationary density modulation are formed with equal amplitudes leading to a density ρ' which is modulated only below its undisturbed value. Analogously, the density change at the location of low field intensity will be modulated only above its equilibrium value. Thus, the total density returns to its undisturbed value once each acoustic period T_a. The diffraction efficiency is proportional to the squared density variation. It is a periodic function that can be decomposed into a superposition of a constant (non-oscillating) term, and two oscillating terms with frequencies ϖ and 2 ϖ, respectively. Since the term with frequency ϖ is dominating, the grating diffraction efficiency displays an oscillation at the acoustic frequency ϖ. Again, since for the experiments described in this work $\varpi \gg \beta_1$, β_2, the amplitude of the oscillating density has been approximated by $L' \approx 1$ and its phase by $\Phi' \approx \pi/2$. The standing acoustic wave induced by instantaneous heat release, i.e., the thermal acoustic wave, is thus $\pi/2$ phase shifted with respect to the standing acoustic wave induced by electrostriction. Now, depending on the ratio of γ_a and γ_e, i.e., the mechanisms that dominate the grating formation, the temporal evolution of the LIG diffraction efficiency will oscillate at the acoustic frequency or at twice the acoustic frequency. If electrostriction and heat release contribute roughly in the same way to the grating formation, the resulting reflectivity will display an oscillation at twice the acoustic frequency with enhancement of every other peak.

If the process of collisional relaxation of absorbed energy is slow compared to the acoustic oscillation period $2\pi/\varpi$, i.e.,

if $\mu \ll \varpi$, Eq. (17) is reduced to

$$\Xi_{\text{therm}}(t) = \frac{\gamma_a \zeta \lambda}{2\varpi\,(\beta_2 - \mu)} \left[e^{-\beta_2 (t-t_0)} - e^{-\mu (t-t_0)} \right]. \tag{23}$$

When heat is slowly released the pressure rise is continuously drained by acoustic waves. The process is nearly isobaric and favors the formation of a stationary density modulation whereas the development of the standing acoustic wave is hindered due to destructive interference.

For the derivation of the laser-induced variations of density and temperature the condition of local thermal equilibrium has been assumed. If this condition is no longer fulfilled, more complex gas kinetic models have to be employed [13, 14].

In the description presented above the temporal behavior of the excitation pulses has been approximated by a δ-function. This approximation is valid as long as the pulse duration τ satisfy the relations $\tau \ll 1/\varpi, 1/\beta_1, 1/\beta_2$.

In the following, a calculation of the more realistic situation of a laser pulse exhibiting a Gaussian temporal profile is given. For simplicity, we consider the case of a pure acoustic wave induced solely by electrostriction. The new source term in the upper equation of system (11) can now be written as

$$\frac{\varepsilon_0 \gamma_e}{2} \nabla^2 \bar{E}_s^2 = -\varepsilon_0 \gamma_e A q^2 \cos(qx) G^2(t) \tag{12'}$$

where $G(t)$ is the Gaussian temporal profile of the pulse

$$G(t) = \frac{\sqrt{2}}{(\tau)^{1/2}\,(\pi)^{1/4}} e^{-\frac{1}{2}\left[\frac{t-t_c}{\tau}\right]^2}, \tag{24}$$

t_c is the position of the maximum of $G(t)$, τ is its width and $G(t)$ is normalized as $\int_{-\infty}^{+\infty} G^2(t)\,dt = 1$.

In the approximation that takes into account only terms linear in β_1/ϖ and β_2/ϖ and neglecting the contribution from the stationary density modulation, the temporally dependent part of the density variation induced by a $\delta(t)$ pulse is, see Eqs. (15) and (16):

$$\rho'_G(t) = \frac{\gamma_e}{2} \frac{\varepsilon_0 A q^2}{\varpi} \Theta(t) \left\{ e^{-\beta_1 (t)} \left[\sin(\bar{\omega}(t)) \right] \right\}. \tag{25}$$

The total density variation induced by a Gaussian pulse is obtained by convoluting the induced density variation caused by a $\delta(t)$ shaped pulse, i.e., $\rho'_G(t)$, with the time dependent part of the new source term, and multiplying by the spatially dependent part, explicitly (for details see [7]):

$$\rho'(x,t) = \frac{\gamma_e}{\sqrt{2}} \frac{\varepsilon_0 A q^2}{\varpi} \cos(qx) \times \mathrm{Im} \left\{ e^c \left[1 + erf \left(\frac{\sqrt{2}}{\tau} (t-b) \right) \right] \right\} \tag{26}$$

with

$$b = t_c + \frac{\tau^2}{4}(\beta_1 - i\varpi)$$

$$c = \frac{\tau^2}{8}(\beta_1 - i\varpi)^2 - (\beta_1 - i\varpi)(t - t_c) \tag{27}$$

and with the error function *erf(x)*, which is defined as

$$erf(x) = \frac{2}{\pi} \int_0^x e^{-y^2} dy \tag{28}$$

Figure 1 shows plots of the temporal behavior of the diffraction efficiency of a pure electrostrictive grating generated with pulses exhibiting a Gaussian temporal profile, as described by Eq. (24). The calculation is performed using Eq. (26) for three different widths τ of the Gaussian excitation pulses, respectively. For this example the acoustic frequency ϖ has been set to 1.5×10^8 s^{-1} corresponding to a grating oscillation period $T_g = 2.1 \times 10^{-8}$ s. Such frequency can be generated in air at 1 bar using e.g., an excitation wavelength of 1064 nm and a crossing angle between the excitation beams of roughly 4°. For the decay rate β_1 the value of 3×10^6 s^{-1} has been used. For τ =5 ns the approximation of delta excitation pulses is correct. This calculated grating diffraction efficiency displays a similar profile as it can be obtained by using Eq. (20). For a slower LIG formation process the generation of a standing acoustic wave is hindered by the destructive interference between the acoustic waves generated at different times during the long excitation pulse. For $\tau \approx T_g$ the first oscillation peak increases while the acoustic oscillations are

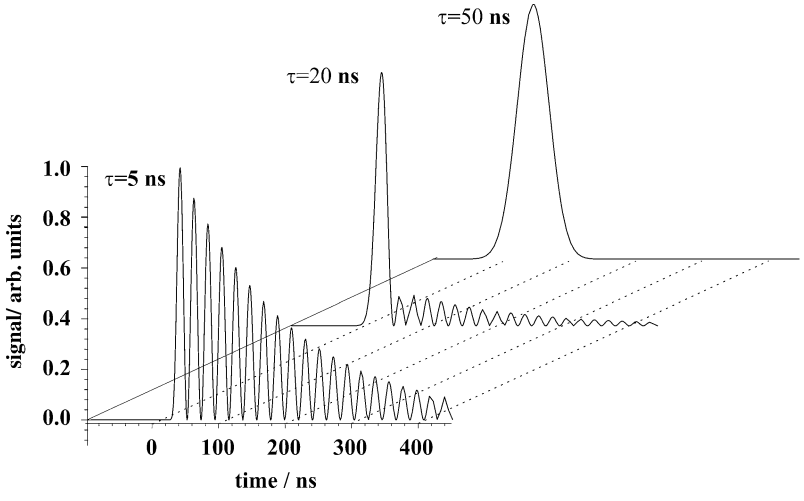

FIGURE 1 Calculated temporal behavior of the electrostrictive LIG reflectivity for different widths τ (τ = 5 ns, τ = 20 ns, τ = 50 ns) of the Gaussian temporal profile of the excitation pulses obtained using Eq. (26)

reduced though still visible. Finally for $\tau > T_g$ only the shape of the excitation pulse is visible indicating that the acoustic waves cancel out completely and the temporal development of the LIG diffraction efficiency follows the excitation pulse.

3 Methodological studies of the technique: Choice of the laser source and of the experimental parameters

One of the findings reported here concerns the choice of the most appropriate optical sources for the set up of the LIG technique used for diagnostics purposes in the gas phase. A powerful pulsed laser to generate the grating, and a cw or pulsed laser to read out the grating are required. Multimode pulsed Nd: YAG lasers, exhibiting approximately ns pulse length, are good candidates owing to their compactness, ease of use, relative low cost and high intensity output. Obviously, care must be taken when setting up an experiment because their characteristics will affect the measurement in some way. The results of the experimental investigation on this issue are reviewed in the following sections. The best experimental configurations for the different applications of the LIG technique for diagnostics, as presented in [1], have been chosen based on these findings.

3.1 *Coherence effects*

Typically, since the coherence time is inversely proportional to the bandwidth, multimode lasers have a short coherence time. For example, a Nd: YAG multimode pulsed laser with a bandwidth of approximately 30 GHz has a coherence time of about 30 ps. The diffraction efficiency η of a grating depends on the time delay τ_d between the two excitation beams. If the duration of the excitation pulses τ is much longer than the coherence time of the excitation laser τ_c one has to account for the time dependence of the excitation fields. The diffraction efficiency of a laser-induced grating depends on the temporal coherence function of the source laser which generates the grating. For example, the signal intensity from an electrostrictive LIG is reduced approximately by a factor τ/τ_c, when using temporally incoherent excitation beams instead of temporally coherent ($\tau_d = 0$) excitation beams when using an excitation source that exhibit a Gaussian statistics of the longitudinal modes, see [4].

The experimental configuration used to investigate the influence of the temporal coherence of the excitation laser on the generated electrostrictive grating signal is described in [4]. The two excitation beams have been generated by a frequency doubled multimode Nd: YAG laser (Continuum NY81-10) with a pulse width of about 5 ns (full width at half-maximum, FWHM). The IR spectral bandwidth of its radiation is specified to be 1 cm^{-1} (FWHM). A variable path length enabled to vary delay between the two excitation beams. The frequency doubled output of a second Nd: YAG laser provided the probe beam, which has been diffracted off the grating into the signal beam. Figure 2 shows a measurement in ambient air of the signal intensity *vs.* the time delay between the two excitation beams. The data have been fitted by a sum of a Gaussian function and a constant. For a delay time of 95–101 ns between the excitation and probe pulses the signal intensity at $\tau_d = 65$ ps (not shown in Fig. 2) has been measured to be smaller by a factor of $(3.0 \pm 0.2) \times 10^2$ compared to the signal intensity at $\tau_d = 0$. This matches fairly well the calculated value $\tau/\tau_c = 4.0 \times 10^2$, see [4].

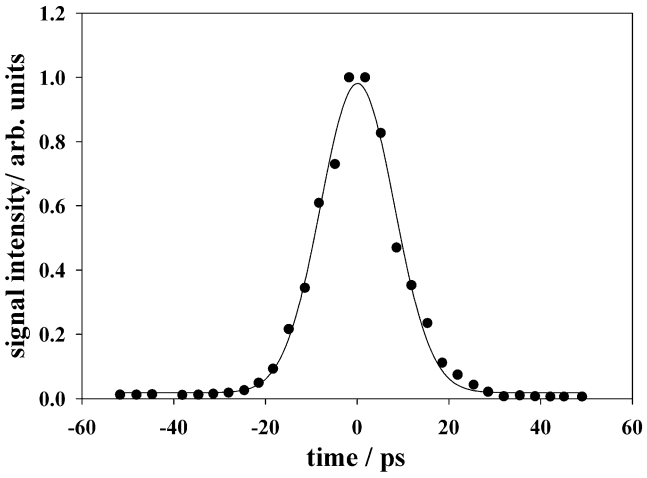

FIGURE 2 Signal intensity of an electrostrictive laser-induced grating generated in ambient air *vs.* time delay τ_d between the excitation beams. The *solid line* is a fit by using the sum of a Gaussian function and an offset

Hence, when using pulsed multimode lasers, it is crucial to reduce the optical path difference of the excitation beams to a small fraction of the coherence length of the laser source in order to obtain high grating diffraction efficiency. This can be achieved by introducing an optical delay line in the path of one (or both) of the excitation beams.

3.2 *Optical breakdown in gases*

The grating diffraction efficiency is proportional to the intensity of the excitation source. Using high intensity excitation beams leads on one side to an increased signal; on the other side it may change the properties of the sample and affects the LIG formation mechanisms. The traces in Fig. 3 show the temporal behavior of a laser-induced grating generated with excitation beams arising from the fundamental output of a Nd: YAG laser at the pulse energies of roughly 90 mJ and 380 mJ, respectively. Both measurements have been obtained in 1 bar argon at room temperature using the experimental setup and beam geometry shown [15] and used for temperature measurements. Approaching the threshold for optical breakdown the temporal signature of the grating reflectivity changes and its oscillation frequency is reduced to half of its initial value, indicating a release of heat in the medium. The energy deposition into the medium through resonant absorption is excluded since the excitation wavelength $\lambda_{exc} = 1064$ nm is far from any transition of argon. In fact, at high laser intensities the mechanisms of energy deposition in the gas occurs in two steps. Initially, electrons may be generated in the gas by multiphoton ionization. Electron avalanche ionization can develop if the initial electrons can gain enough energy from the laser field to ionize an atom in collisions. Repetition of the process can lead to a rapid multiplication of the number of electrons. From the requirement of energy and

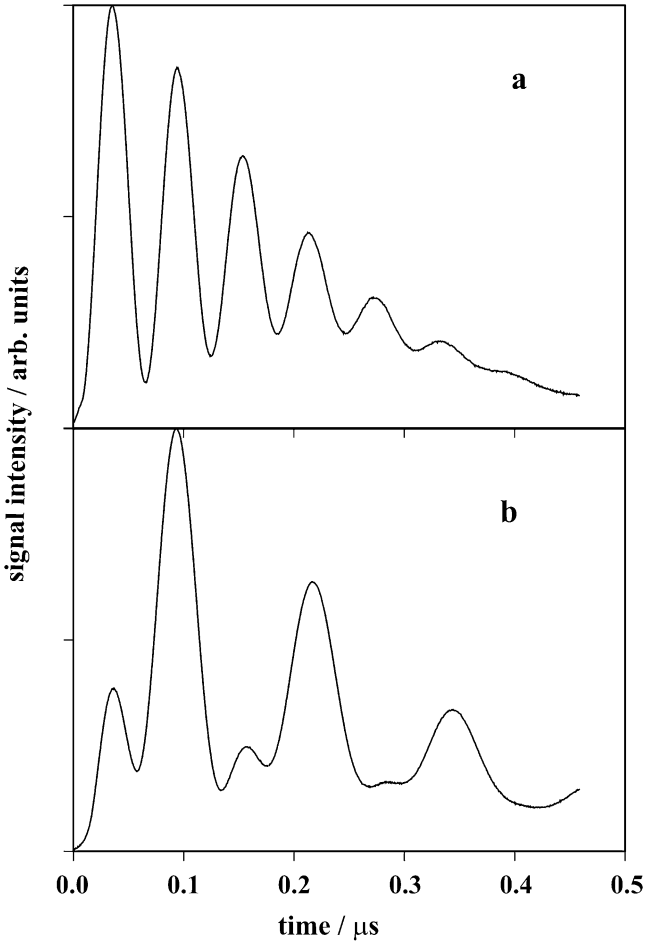

FIGURE 3 Temporal behavior of a laser induced grating generated in argon at atmospheric pressure and ambient temperature. The excitation beams have a wavelength $\lambda_{exc} = 1064$ nm, a diameter of roughly 6 mm and are focused by a 750 mm focal length lens to intersect at an angle of 1.6°. The probe beam arises from an cw Ar^+ laser at $\lambda_{pr} = 514.5$ nm. The phase matching condition (Bragg condition) of the three beam is achieved in a 3D forward geometry. **a**: signal obtained with roughly 90 mJ/ pulse excitation laser energy; **b**: signal obtained with roughly 380 mJ/pulse excitation laser energy

momentum conservation, an electron can absorb a photon only if it is colliding with an atom or ion. The electrons in the laser field will gain kinetic energy through electron-neutral inverse Bremsstrahlung collisions [16, 17] (this is the inverse of the Bremstrahlungs process in which high energy electrons, upon traversing a gas emit radiation as they slow down). The accelerated electrons will lose their energy by elastic and inelastic collisions with neutral atoms through excitation of external (i.e., translational) and internal (e.g., electronic) degrees of freedom of the atoms. In this way the radiation energy is "absorbed" by the gas, which is locally heated resulting in the formation of a thermal grating. Figure 3a shows the situation where a pure electrostrictive grating oscillating at twice the acoustic frequency has been generated, while in Fig. 3b the transition to a thermal grating oscillating at the acoustic frequency is clearly visible. No attempt has been made to quantify this effect. Nevertheless laser-induced gratings show a potential to investigate the behavior of gases at the threshold of optical breakdown. On the other hand, these findings underline the necessity to account for the excitation pulse energies for a correct interpretation of the results obtained by using the LIG technique.

3.3 *The read-out beam source*

The choice of the pump beam source depending on its characteristics and their influence on the generated grating has been described so far. This section is dedicated to the reasons rendering an Ar^+-laser the most suitable read out source. The most important advantage of probing the grating with a cw-laser, combined with a time resolved acquisition, is the possibility of detecting the temporal behavior of the transient grating over the complete range of its life time by a single-shot measurement. Using a pulsed probe beam to read out the grating, as described in [4], an electronic delay between the probe beam and the grating beams is required in order to scan over the entire range of the grating lifetime. In this way every measured point of the recorded temporal evolution of the signal arises from a different pulse of the excitation laser and of the probe laser. Thus, no single shot measurement of the signal temporal evolution over the entire grating lifetime range is possible. Furthermore, to perform a measurement over the life time range of the grating can be very time consuming and variations of the laser characteristics occurring during this time will also affect the signal rendering its interpretation more difficult. Note that the signal obtained with an intense pulsed probe beam (some MW/pulse) is much stronger than a typical cw readout (about 1 W). This latter signal is nearly a single photon event. Despite the high number of photons per pulse no statistical advantage results from using a pulsed probe beam because there is no correlation between the measured data points over the range of the LIG lifetime, since they have been recorded with different excitation and different probe pulses. Furthermore, the modulation depth of the signal oscillations is enhanced for a cw probe beam as compared to a pulsed probe source. In fact, the measured signal is the convolution of the three following functions: The temporal profiles of the grating diffraction efficiency and of the probe beam, respectively, and the time response function of the detection system. For a cw read out of the grating the signal is simply the convolution of the temporal response of the grating diffraction efficiency with the time response of the detection system thus leading to an enhanced modulation amplitude. This effect is visible in Fig. 4a which shows the temporal evolution of the signal obtained by diffracting a pulsed probe beam off an electrostrictive LIG generated in argon at 5 bar and ambient temperature. In Fig. 4b a cw-probe beam has been employed to perform a single-shot measurement of the temporal evolution of the electrostrictive LIG. Comparison of the signals depicted in Fig. 4a and in Fig. 4b shows that the modulation depth of the oscillation of the signal is more pronounced for a cw read-out of the grating. The higher modulation depth is an advantage for the fitting of the results, especially in the case of small oscillation periods of the LIG diffraction efficiency (which are comparable to the duration of the excitation pulses). Figure 5 shows plots of the calculated signals for two different width τ_1 of the read out

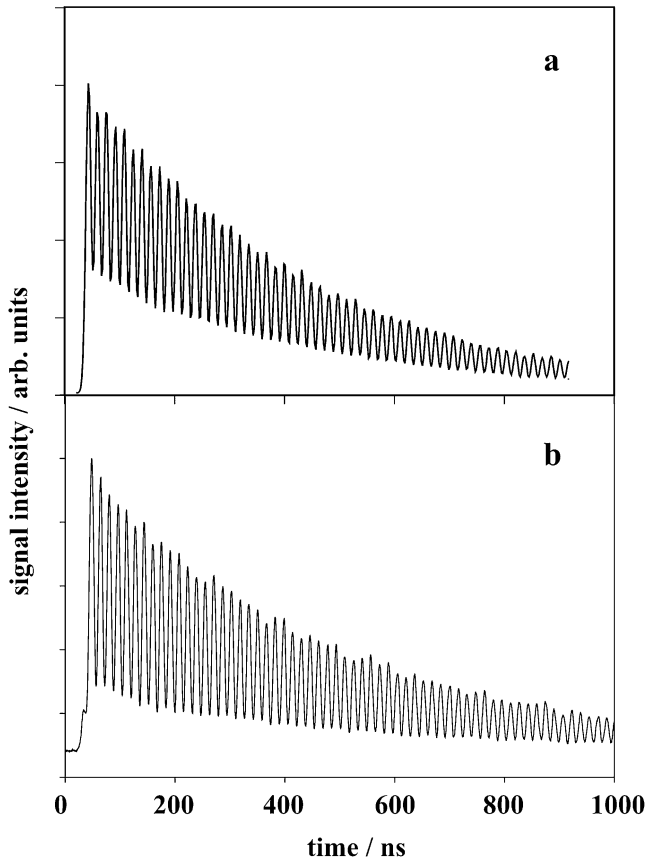

FIGURE 4 Temporal behavior of an electrostrictive laser-induced grating generated in argon at 5 bar and ambient temperature. A planar geometry with unfocused beams and an excitation beams intersection angle of about 3° is used. **a**: probe beam from a pulsed Nd: YAG laser, every measurement is averaged over 100 laser shots. **b**: probe beam from an Ar^+ laser, signal is averaged over ten laser shots

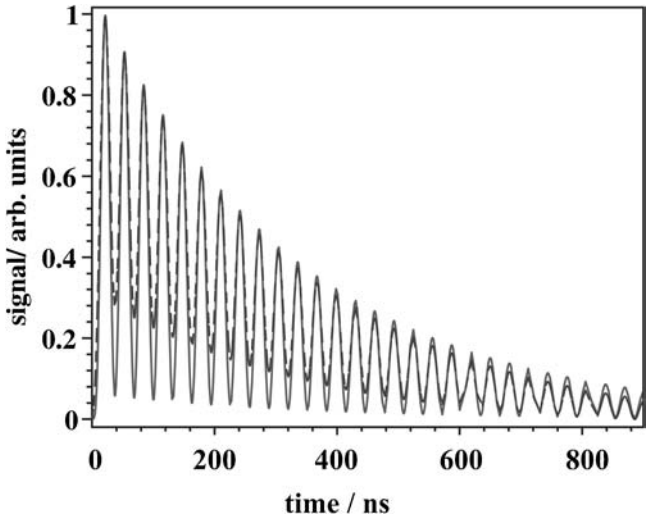

FIGURE 5 Calculated temporal behavior of a pure electrostrictive LIG signal for different widths τ_1 of the Gaussian readout pulse obtained using Eqs. (14) and (15). $\tau_1 = 3.5$ ns (solid), $\tau_1 = 8$ ns (dashed)

pulse. The signals were obtained convoluting the diffraction efficiency for a pure electrostrictive grating (see Eqs. (14) and (15)) and a Gaussian which has been assumed to describe the temporal behavior of the read out pulse. Comparison of the traces in Fig. 5 shows that the modulation decreases with increasing width of the read out pulse as expected. For this example the acoustic frequency ω has been set to 1×10^8 s^{-1} corresponding to a grating oscillation period $T_g = 31$ ns and β_1 is 1.5×10^6 s^{-1}.

3.4 *Sound propagation effects made visible by the alignment of the beams and their spatial intensity profiles*

Since the LIG diffraction efficiency scales with the intensity of the pump beams, the signal intensity is expected to increase for a tighter focusing of the beams. Additionally, the size of the probe volume represents another important feature of any optical diagnostics approach since it defines the spatial resolution which is achievable. The latter is particularly important for experiments in inhomogeneous media or in the presence of turbulences. The size of the interaction volume is determined by the overlap of the excitation and the probe beams [8]. Focusing the beams reduces the interaction volume and may increase the signal intensity. On the other hand, it causes an increase of the decay rate of signal amplitude since the sound wave packet leaves the probed volume more rapidly. Sometimes the decay of the signal is predominantly due to the latter effect. In the following the issue on the different mechanisms causing the decay of the LIG signal is addressed.

Figure 6 shows the temporal evolution of two electrostrictive laser-induced grating signals generated with different intensity cross sections of the excitation beams. For these experiments, the excitations beams are obtained from the fundamental output of a pulsed Nd: YAG laser while the probe beam is generated by using a cw Ar^+ laser. The two excitation beams are crossed by a 750 mm focal length lens and the phase matching condition of the three beams is realized in a planar backward geometry.

Figure 6a shows the temporal evolution of a grating generated by using excitation beams with a Gaussian intensity profile of about 6 mm diameter (at $1/e^2$ level of the maximal intensity) at the focusing lens. The measurement depicted in Fig. 6b is obtained using excitation beams having a strip shaped intensity profile. To obtain such an intensity cross section the Nd: YAG beam passed through a cylindrical Galilean telescope before being split into two beams. In this way two excitation beams with very tight elliptical intensity profiles (stripes) of about 6 mm height and 1 mm width are obtained at the focusing lens. Due to diffraction the heights of the stripes are focused tighter than their widths by the lens and result in a strip-shaped focus of approximately 1 mm width and 160 μm height. The orientation of the strip-shaped cross sections has been chosen such that the direction of their larger extension coincides with the propagation direction of the induced acoustic waves. The signal in Fig. 6b displays a remarkable number of additional oscillations and a longer grating lifetime compared to the signal in Fig. 6a obtained without shaping intensity cross section of the excitation beams. Using $v = 347$ m/s for the sound velocity in air at 1 bar and room temperature, the acoustic waves would require about 3 µs to completely leave the interaction volume. On the other hand, the grating lifetime is also limited by the damping of the acoustic wave which is characterized by a decay time of the order of 1 µs for these experimental conditions, see

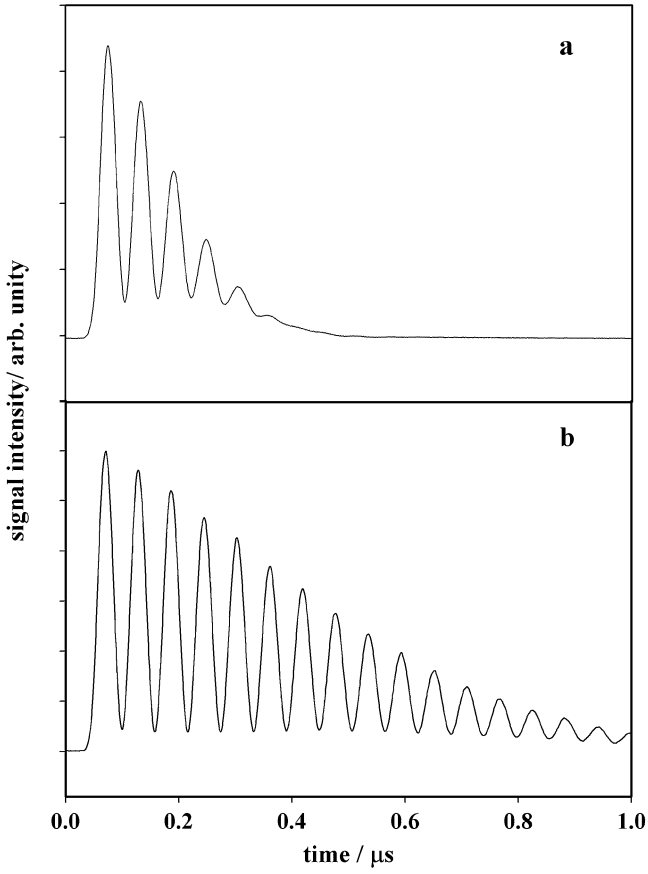

FIGURE 6 Temporal behavior of an electrostrictive laser-induced grating in air at room temperature and atmospheric pressure, generated with $\lambda_{exc} = 1064$ nm and $\lambda_{pr} = 514.5$ nm. The excitation beams are crossed by using a 750 mm focal length lens at an angle $\theta = 1.5°$. **a**: the intensity profile of the excitation beams is Gaussian, with a diameter of 6 mm ($1/e^2$ FWHM); **b**: signal generated with excitation beams exhibiting strip shaped intensity profiles

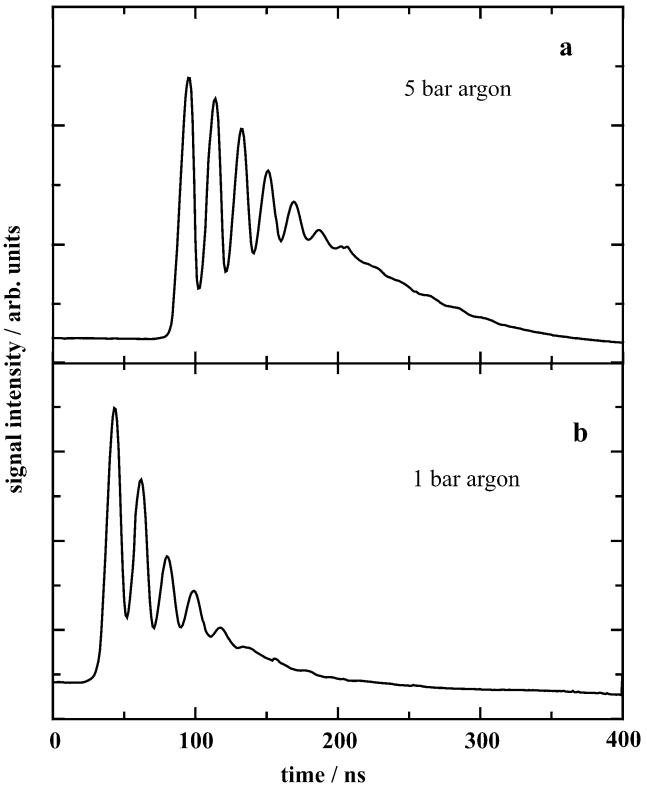

FIGURE 7 Temporal behavior of an electrostrictive grating generated in argon at room temperature **a**: at 5 bar and **b**: at 1 bar. Both measurements are performed using a 3D-forward phase matching geometry with excitation beams at 532 nm of 6 mm diameter focused by a 400 mm focal length lens at an angle of about 3° and a probe beam from a cw Ar^+ laser at 514.5 nm. Both signals are averaged over 100 laser shots

Eqs. (15) and (19). In this case, the damping of the acoustic wave is dominating over the decay of the generated grating. The situation is different for excitation beams having a circular intensity profile of about 6 mm diameter, which are focused by a 750 mm focal length lens. The acoustic waves leave the overlap volume completely, exhibiting a dimension of about 170 μm, after roughly 500 ns, rendering the damping of the acoustic wave unimportant. Therefore, in this case the propagation of the acoustic waves out of the interaction region is the dominant factor limiting the grating lifetime. To account for the faster decay of the standing acoustic wave one can phenomenologically include an additional factor, f_d, in the temporal evolution of the diffraction efficiency [9, 18]

$$f_d = \exp\left(-\frac{4v_s^2 t^2 \cos^2\theta/2}{w^2}\right) \equiv \exp\left(-\frac{2t^2}{\tau_{tr}^2}\right) \qquad (29)$$

where w denotes the beam waist (1/e level) of the excitation beams at their focus. The acoustic transit time, denoted by τ_{tr}, describes the decay of the LIG diffraction efficiency due to the relative displacement of the counter-propagating acoustic waves.

In summary, using excitation beams with a strip shaped intensity profile enables to achieve a good spatial resolution, high intensity signal and reduces the effect of acoustic waves propagating beyond the limits of the probed volume.

In the following, a description of further situations is given where the effect of sound propagation is visible. An acoustic wave causes a non-oscillating contribution to the LIG signal intensity, which grows and decays concomitantly with the oscillatory part. The temporal growth of this contribution leads to a reflectivity that is increasingly less modulated. A comparison between the traces obtained in Ar at 5 and 1 bar shown in Fig. 7a and b, respectively, clearly illustrates this behavior. Even though the dissipation of the acoustic wave is considerably smaller at 5 bar, the number of visible peaks remains roughly the same as compared to the 1 bar example. The non-oscillating part of the LIG diffraction efficiency, however, decays much slower at 5 bar.

The accuracy of the geometrical alignment of the three beams represents an additional parameter which affects the modulation depth of the signal. If the three beams are perfectly aligned in order to satisfy the Bragg condition, the probe beam scatters mainly from the center of the overlap volume of the three beams where the standing acoustic wave is pervasive. A slight misalignment of the beams, however, results in poor interference of the counter-propagating acoustic waves and, therefore, to the presence of additional propagating acoustic waves in the center of the overlap region. As a consequence, the signal generated in this region displays a slowly varying background resulting from the scattering of the probe beam

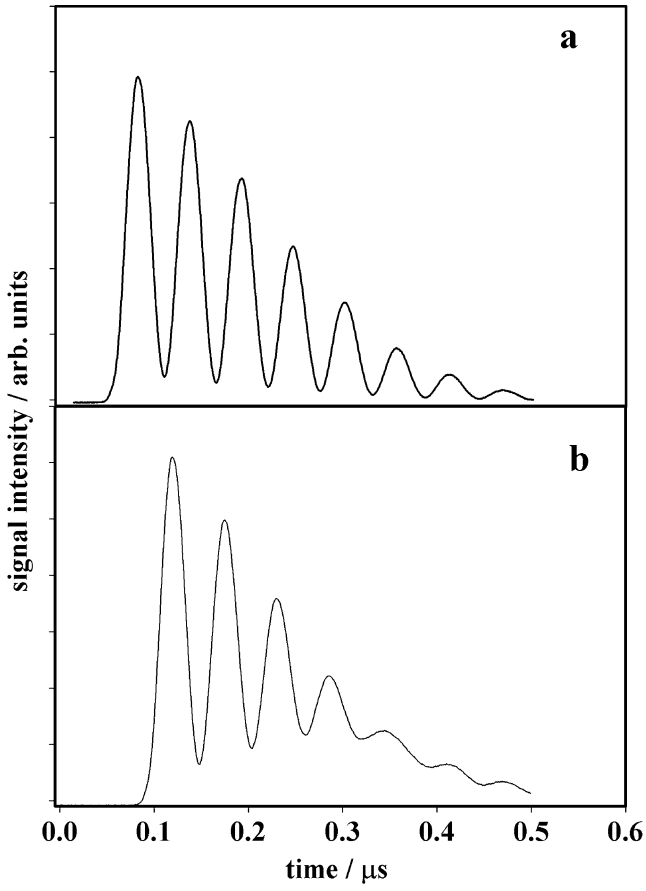

FIGURE 8 Electrostrictive grating signals obtained with **a**: carefully aligned beams and **b**: with slightly misaligned beams, respectively. Both signal are generated in air at atmospheric pressure and ambient temperature. The beam geometry is planar with an intersection angle of the excitation beams of 1.5°. The wavelength of the excitation beams is 1064 nm. The probe beam arises from a cw Ar^+ laser at 514.5 nm. All the beams have a circular intensity cross section with approximately the same diameter. Both signals were averaged over 100 laser shots

off the propagating acoustic wave concurrently with the oscillating signal from a standing acoustic wave. This effect is visible when comparing the signal shown in Fig. 8a, obtained with carefully aligned beams, and the signal displayed in Fig. 8b resulting from slight misalignment of the beams. For this measurement, the excitation beams have been arranged in order to intersect prior their focal point while keeping the position of the probe beam unchanged. For both measurements, the signal arising from the center of the overlap region has been recorded by introducing a diaphragm aperture of about 4 mm. The beam geometry is backward planar with excitation beams intersecting at an angle of the of 1.5°, an excitation wavelength at 1064 nm, a probe beam from a cw Ar^+-laser at 514.5 nm and a circular intensity cross section of approximately the same diameter for all the beams. Both signals have been averaged over 100 laser shots and have been generated in air at atmospheric pressure and ambient temperature.

Furthermore, a contribution to the signal temporal evolution caused by sound propagation might also occur due to size effects of the probe beam. The signal oscillations mirror the oscillations of the standing acoustic wave resulting from the superposition of the counter-propagating acoustic waves. With increasing time the acoustic wave packets propagate out of the overlap volume in directions perpendicular to the grating planes. Thus, the resulting standing acoustic wave will be more and more confined to the center of the overlap volume.

Eventually, the standing acoustic wave disappears completely when the propagating acoustic waves no longer overlap. Subsequently, only propagating acoustic waves will be present in the overlap region. One can distinguish between two situations: either the probe beam waist w_{pr} is smaller or larger than the spot size of the overlap region w_{exc}, see. [8]. Using excitation beams exhibiting a strip-shaped intensity profile corresponds to the situation when $w_{pr} \ll w_{exc}$. Explicitly, the waist of such excitation beams in the overlap region (i.e., in their focus) is approximately 1 mm in the direction of the propagation of the acoustic waves while the Ar^+ beam's waist is about 100 μm. Therefore, the signal obtained with such beams comprises contributions generated at both, the center and the periphery of the overlap region. For a selective observation of these contributions an iris diaphragm with a variable aperture has been placed in front of the photo-multiplier tube. Its position is arbitrarily shifted in height and in width perpendicularly to the direction of propagation of the signal beam. For the measurement shown in Fig. 9a, the iris diaphragm

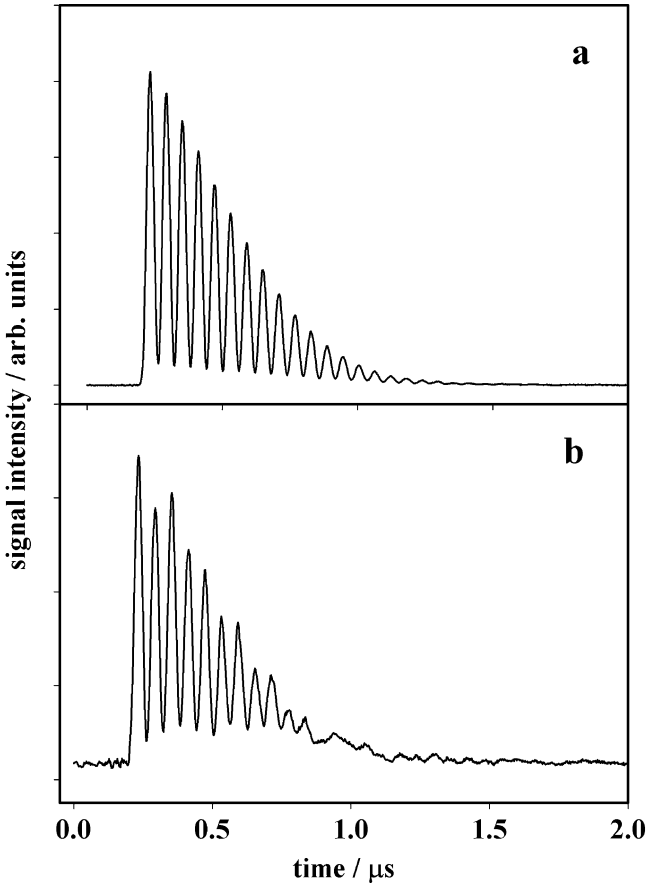

FIGURE 9 Temporal behavior of a laser induced electrostrictive grating generated in air at ambient conditions. Signal arising from **a**: the center of the overlap volume and **b**: 3 mm apart from the center. The measurements were performed using excitation beams from a Nd:YAG laser at 1064 nm intersecting at an angle of about 1.5° and a probe beam from an Ar^+ laser at 514.5 nm arranged in a planar backward beam geometry. Every measured point is averaged over 100 laser shots

with an aperture of about 4 mm has been placed at the center of the scattered beam. Alternatively the diaphragm has been shifted 3 mm aside keeping the height and all other experimental parameter unchanged. The result of this measurement is shown in Fig. 9b. Besides a reduction of the signal intensity a contribution from the propagating wave is visible as a slowly varying background leading to a reduction of the oscillation modulation.

In summary, the presence of a slowly varying background in the temporal evolution of the LIG diffraction efficiency may be caused by a misalignment of the beams or by the small dimensions of their interaction volume. Tight focusing of the beams combined with high pressure of the gas renders this effect even more visible.

4 Summary and conclusions

The present paper is devoted to understanding the formation mechanisms of transient electrostrictive and thermal LIGs generated in the gas phase. Laser induced gratings arise from the interaction between matter and the light of an interference structure of two crossed laser beams. This interaction leads to a spatially periodic modulation of the refractive index of the material in the overlap region of the two crossed beams. This grating-like structure can be detected by diffracting a third beam off the laser induced refractive index modulations. The characteristics of the diffraction efficiency of such gratings depend on their formation mechanisms. In Sect. 2, the explicit calculation of the LIG diffraction efficiency for the different formation mechanisms is given. For this purpose, the linearized hydrodynamic equations have been solved and the following results have been obtained. Electrostriction generates mainly a standing acoustic wave, and in addition a small amplitude stationary density wave. Since the grating diffraction efficiency is proportional to the squared density change, the electrostrictive grating diffraction efficiency oscillates at twice the acoustic frequency. Release of the absorbed laser radiation in form of heat through collisions leads to the formation of a thermal grating which comprises the contribution of both a standing acoustic wave and a stationary density modulation. The rate of the heat exchange process governs the amplitudes of these contributions as well as the characteristics of the temporal behavior of the induced thermal grating. Instantaneous heat release forms a standing acoustic wave and a stationary density modulation of equal amplitude. The diffraction efficiency of a thermal grating displays an oscillation at the acoustic frequency. When the absorbed radiation energy is slowly released a stationary density modulation contribution is dominant and the grating diffraction efficiency displays a slowly varying hump.

In Sect. 3, the influence of various parameters on the generated electrostrictive or thermal grating such as the laser beam size, the characteristics of the LIG read out source (pulsed or cw), the pressure, the laser intensity, and the coherence length of the excitation laser have been measured. These data provide, on one hand, a test of the theoretical model. On the other hand, they consent to design the optimal experimental configuration depending on the specific application of the technique. Furthermore, these investigations reveal some limitations of the technique. In this context, the possibility to apply LIG to investigate optical breakdown in gases has been demonstrated qualitatively in addition.

All these findings have been experimentally verified in a series of carefully designed experiments and used for the analysis of the data obtained for the diagnostics in the gas phase [1].

ACKNOWLEDGEMENTS Helpful discussions with PD M. Spira are gratefully acknowledged. ASP thanks Prof. M. Landolt for stimulating and supporting this work. Financial support has been granted by the Swiss Federal Office of Energy (BEW).

REFERENCES

1 A. Stampanoni-Panariello, D.N. Kozlov, P.P. Radi, B. Hemmerling, Appl. Phys. **B** (2005), DOI 10.1007/s00340-005-1853-y
2 H.J. Eichler, P. Günter, D.W. Pohl, *Laser Induced Dynamic Gratings* (Springer, Berlin, 1986)
3 I.L. Fabelinskii, *Molecular Scattering of Light* (Plenium Press, New York, 1968)
4 A.C. Stampanoni-Panariello, B. Hemmeling, W. Hubschmid, Phys. Rev. **A 51**, 655 (1995)
5 W. Hubschmid, B. Hemmerling, A. Stampanoni-Panariello, J. Opt. Soc. Am. **B12**, 1850 (1995)
6 W. Hubschmid, B. Hemmerling, Chem. Phys. **259**, 109 (2000)
7 A. Stampanoni Panariello, *Laser-Induced Gratings in the Gas Phase: Formation Mechanisms and Applications for Diagnostics*, Series in Quantum Electronics **31** (Hartung-Gorre Verlag, 2003)
8 A.E. Siegman, JOSA **67**, 545 (1977)
9 H. Latzel, T. Dreier, M. Giorgi, R. Fantoni, Ber. Bunsenges. Phys. Chem. **101**, 1065 (1997)
10 R.W. Boyd, *Nonlinear Optics* (Academic Press, New York, 1992)
11 P.H. Paul, R.L. Farrow, P.M. Danehy, J. Opt. Soc. Am. **B12**, 384 (1995)
12 B. Hemmerling, D.N. Kozlov, Chem. Phys **291**, 213 (2003)
13 F. Hanser, W. Koller, F. Schürrer, Phys. Rev. **E 61**, 2065 (2000)
14 J.H. Grinstead, P.F. Barker, Phys. Rev. Letts. **85**, 1222 (2000)
15 A.C. Stampanoni-Panariello, B. Hemmerling, W. Hubschmid, Appl. Phys. **B 67**, 125 (1998)
16 T.P. Hughes, *Plasmas and Laser Light* (Adam Hilger, 1975)
17 G. Bekefi (ed.), *Principles of Laser Plasmas* (Wiley, 1976)
18 D.N. Kozlov, B. Hemmerling, A.C. Stampanoni-Panariello, Appl. Phys. **B 71**, 585 (2000)